UNIVERSAL WISER
PUBLISHER

Article

Open-Source Data Processing Chain for Marche Region X-band Weather Radar

Francesco Iocca[1], Marco Lazzeri[1] and Marco Pellegrini[2,3,*]

[1]Functional Centre, Marche Region Civil Protection Service, 60126 Ancona, Italy
[2]LIF Srl, 50018 Scandicci (Firenze), Italy
[3]Department of Life and Environmental Sciences (DISVA), Università Politecnica delle Marche, 60131 Ancona, Italy
E-mail: marco.pellegrini@ieee.org

Abstract: In the framework of three projects co-funded by the European Union (EU), an X-band (8-12 GHz frequency range) polarimetric radar was installed in the Marche Region territory (East-Central Italy) at Cingoli municipality, province of Macerata. The radar site is located at about 750 m above sea level and about 30 km away from the Adriatic Sea. The radar, managed by the Marche Region Civil Protection Service, is employed for weather monitoring purposes and is in pre-operational stage. It is known that radar measurements are affected by various sources of error, to be addressed in order to improve the accuracy of final products. Among these, the most important are radar calibration, ground and sea clutter, beam blockage, rain attenuation, wet-radome attenuation, beam-broadening, non-uniform beam filling, vertical variability of precipitation and wireless local-area-network (WLAN) interferences. Nowadays quantitative rainfall estimation using X-band weather radar are essential to meet requirements for flood forecasting, water management and many hydro-meteorological applications. Besides higher resolution, X-band radars are cost-effective compared to S- or C-band radars because of smaller antenna size. On the other hand, main disadvantages of such systems are the large influence of attenuation by liquid water and a relatively short range. In this work, we will present the data-processing chain developed ad hoc in order to remove or at least reduce the sources of error affecting Cingoli radar data. The performance of the data-processing chain was evaluated in the light of case studies related to meteorological events that interested Marche region territory in the last two years. The software was developed using open source technology. The current version of the chain does not take into account the echoes from sea clutter and the attenuation due to wet radome that can be significant at X-band; such issues will be addressed in a future work.

Keywords: X-band weather radar, data processing, open-source software

1. Introduction

Radars at different frequencies have been used over many decades for weather purposes. In particular, conventional S- and C- band systems are employed for long-range coverage observations while dual-polarization X-band radars are useful for networked applications [1]. In recent years, because of smaller antenna size, low-cost X-band radars have been employed to observe local weather phenomena and used for flood forecasting [2–4]. Compared to large and expensive S- and C-band systems, X-band radars cover a smaller area but with a higher spatio-temporal resolution [5] and are strongly affected by attenuation due to atmospheric liquid water [6].

An X-band polarimetric radar was installed at the Cingoli site in the framework of three projects co-funded by the EU. Combined with satellite data, weather forecasting numerical models and lightning detection data, Cingoli radar data is used by the Marche Region Civil Protection Service for weather monitoring purposes.

ADRIARadNet (https://cetemps.aquila.infn.it/adriaradnet), acronym of ADRIAtic integrated RADar-based and web-oriented information processing system NETwork, was a project co-funded by the EU Instrument for Pre-Accession Assistance (IPA) that aimed to support hydro-meteorological monitoring and civil protection decisions. Marche Region Civil Protection Service was one of the project partners. ADRIARadNet, which ran from 2012 to 2015, aimed at creating an innovative Decision Support System (DSS) in order to enhance the response capacity to extreme weather events affecting the security of people in the Adriatic areas. Among ADRIARadNet objectives, the one related to the present work was testing of low cost weather radar systems, combined with satellite data processing systems and conventional ground networks sensors, for Adriatic severe weather monitoring. A first installation of the Marche Region X-band weather radar was carried out in 2014 in the framework of the ADRIARadNet project. The radar was manufactured by ELDES Company, Italy.

CapRadNet (http://cetemps.aquila.infn.it/capradnet), acronym of CAPitalization and exploitation of RADar-based infrastructure and decision support system for environmental hazard management NETwork in the Adriatic and Ionian region, was a project co-funded by the EU IPA Adriatic CBC (Cross Border Cooperation) Programme during 2016. The project aimed at extending the DSS capability designed in the framework of ADRIARadNet to face hazard mitigation taking into account maritime, coastal, airport and metropolitan environments. Low cost weather radar systems, combined with mesoscale numerical weather prediction systems, were used to improve the management of severe weather events on airport flight operations.

Stream (https://www.italy-croatia.eu/web/stream) is a project funded by the Interreg Italy-Croatia CBC Programme, European Regional Development Fund, during the years 2020-2023. Marche Region, one of the project partners, has stipulated an agreement with CETEMPS (Center of Excellence for Telesensing of Environment and Model Prediction of Severe events) at University of L'Aquila (Italy) for realizing some of the objectives foreseen in the Stream project and related to Marche Region X-band weather radar.

The extraction of reliable and meaningful information from radar returns is a complex task and quite often depends on the desired application [7] and in particular on specific radar site and visibility, beam blocking, presence of radio interference as well as ground and sea clutter. The clutter correction provided by the radar vendor and based on proprietary Doppler filtering is not sufficient to eliminate all the sources of unwanted radar echoes for Cingoli site. For this reason, in this work we present the data-processing chain developed ad hoc in order to implement techniques for attenuation correction, removal of clutter and radio interferences, together with the generation of standard precipitation products and the development of a nowcasting product for identification and tracking of storm cells.

In the last decade, a number of initiatives towards a more open weather radar science have been proposed [8]; some relevant examples are BALTRAD (written in a mixture of C/C++, Python and Java) [9] and Python-based libraries wradlib [10] and Py-ART [11]. For the present work we chose free high-level programming language Python since it is easier to integrate in an existing processing chain than BALTRAD and free wradlib library in particular as it is mostly data agnostic [7], i.e., it can process data in multiple formats or from multiple sources. The software was developed as a "wrapper" of wradlib. The effectiveness of the proposed data-processing chain was evaluated in the light of case studies related to meteorological events that recently interested Marche Region territory.

2. Radar Description and Scanning Strategy

Figure 1 shows the territory of Marche Region highlighted in red (on the left) and the position of the radar site (on the right). Cingoli radar covered by radome and its placement on the tower at about 20 m above the ground are shown in Figure 2. While in Figure 3, a picture of the radar on the tower without its radome is reported. Main technical characteristics of Cingoli dual polarization X-band radar are listed in Table 1.
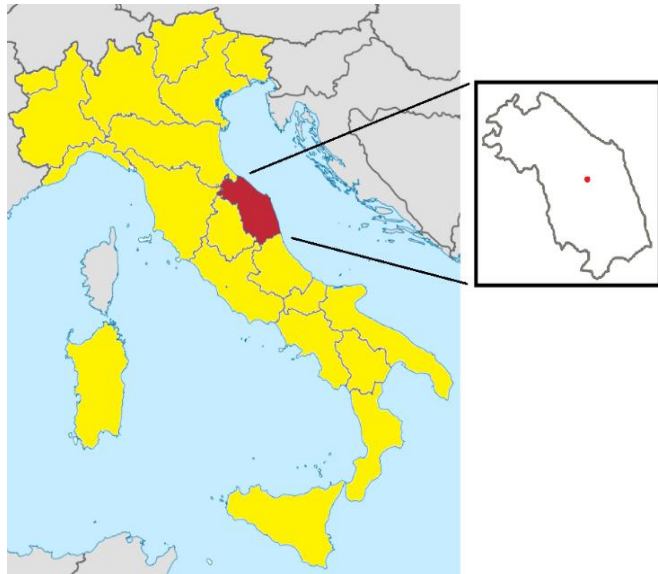
Figure 1. Territory of Marche Region (in red on the left) and a zoom with the position of the Cingoli radar site (on the right).

Figure 2. Cingoli radar covered by radome and its placement on the tower.
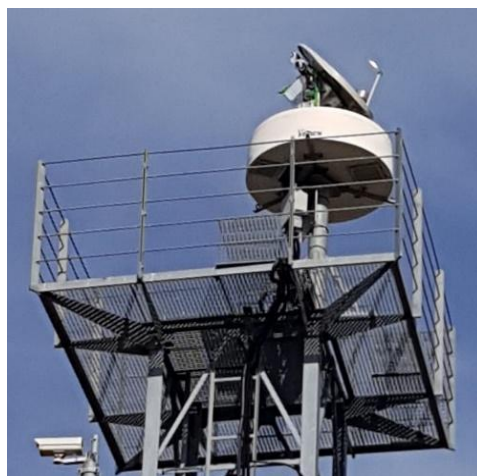
**Figure 3.** Cingoli radar on the tower without the radome.

Table 1. Technical characteristics of Cingoli radar.

Parameter/Characteristic	Value
Vendor	ELDES srl Company, Italy
Frequency	9.41 GHz
Polarization	Dual polarization (Horizontal, Vertical)
Peak power	25 kW (Magnetron) with half power on each channel (H,V)
Antenna type	Offset Cassegrain with elliptical reflector 80 x 90 cm, protected by radome
Overall dimension	Radome with base diameter 123.5 cm and 143 cm height
Weight	< 150 kg (excluded mast)
Antenna Gain	35 dB
Antenna beamwidth	3 degrees
PRF (pulse repetition frequency)	Selectable: 1000 - 750 - 500 Hz
Pulse Width	Selectable: 0.2 - 0.4 - 0.8 μs
Data Format	MSM (ELDES proprietary binary format)
Main radar moments	UZ_H, UZ_V, Z_H, Z_V, V, W, Z_{DR}, Φ_{DP}, ρ_{HV}, SNR
Vendor clutter correction	Doppler filtering
Receiver	Linear digital for simultaneous dual polarization, 14 bit A/D converter
Sensitivity	6 dBZ @ 25 km; 22 dBZ @ 120 km
Dynamic range	> 90 dB

Parameters of the operational volumetric scan for the Cingoli radar are reported in Table 2 and in Figure 4 a representation of the radar beam for 0° elevation and 50° azimuth is shown together with the beam-blocking fraction; Figure 4 was created using a Digital Elevation Model (DEM) of Marche region territory with resolution 100 m. We chose polar coordinates centered on the radar only for Figure 4 in order to highlight the distances relative to Cingoli site and the maximum radar range (120 km) in particular.

Table 2. Main parameters of operational volumetric scan for Cingoli radar.

| Parameter	Value
Scan repeat time	5 minutes
Pulse repetition frequency (PRF)	500 Hz
Elevation(s)	0, 1, 2, 3, 4, 5, 10, 15, 25 degrees
Gate resolution	125 m (0.8 μs pulse width)
Azimuth scan rate	20 degrees per second
Angular scan resolution	1 degree
Angle measurement accuracy	0.25 degrees
Maximum range	120 km (30 km for the last elevation)
Number of integrated pulses	256
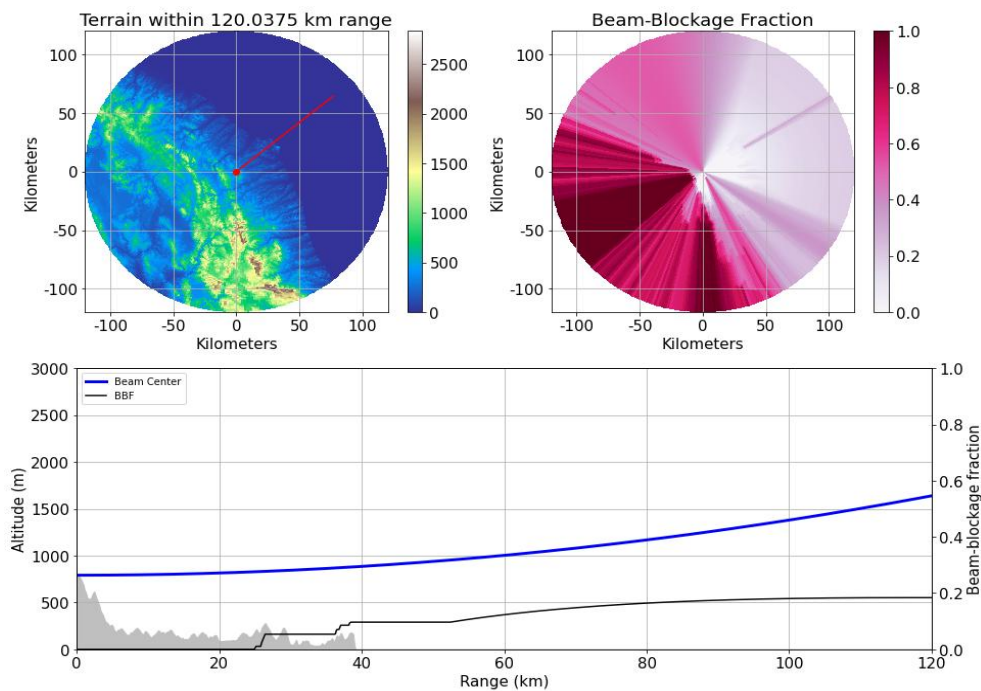
Figure 4. Representation of the radar beam blocking for 0° elevation and 50° azimuth.

The definition of the operational scan has undergone changes over time and the choice of parameter values was made taking into account the fact that Cingoli radar is used by the Civil Protection Service for meteorological monitoring purposes. The first operation carried out for this work was converting volumetric radar data from the proprietary Eldes binary format (called MSM) into HDF5 (Hierarchical Data Format version 5) files which conform to the ODIM (OPERA Data Information Model) standard (http://www.eumetnet.eu/opera). ODIM is an information model for use with weather radar data and products [12]. All the filtering operations described here have been performed on volumetric radar data in polar format. Filtering the data in polar format has made it possible to considerably reduce the calculation times compared to processing the interpolated data. Radar data is interpolated on a regular Cartesian grid only at the end of the whole filtering chain in order to easily display standard products such as Vertical Maximum Intensity (VMI), Constant Altitude Plan Position Indicator (CAPPI), Surface Rainfall Intensity (SRI) and Surface Rainfall Total (SRT).
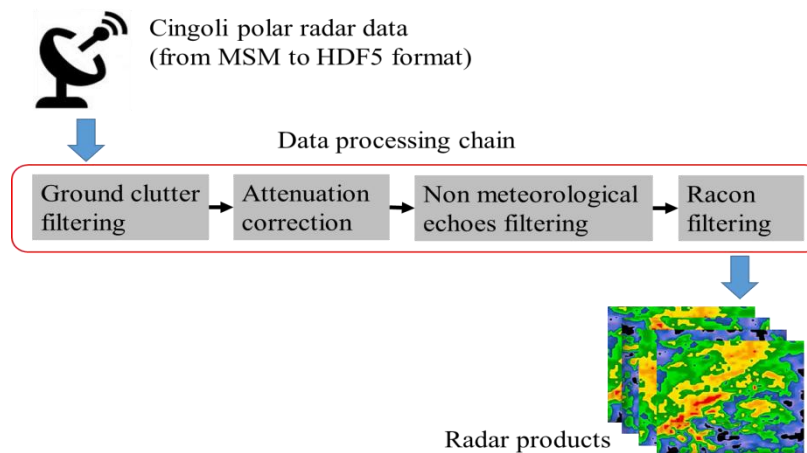
3. Cingoli Radar Data Processing Chain

This section details Cingoli radar data processing chain; in order to show the performance of the algorithms used, radar data is presented before and after filtering operations. As an example, we report data measured by the Cingoli radar on 2021-7-19 at 1:30 UTC at the lowest elevation in presence of precipitation; in particular, Figure 5 shows the unfiltered horizontal reflectivity (UZ_H) on the left and horizontal reflectivity Doppler-filtered by Eldes (Z_H) on the right. Note that in July 2019 Cingoli radar scan consisted of seven elevations whose lowest angle was set at 1.5°. In addition to the weather feature (labeled as A in Figure 5), UZ_H data clearly shows the presence of ground clutter mostly due to Apennine chain (labeled as B), radio interferences (labeled as C), RACON (RAdar beaCON) echoes (labeled as D) and clutter from the Adriatic Sea (labeled as E). From Figure 5 onwards, radar plots for this work have been created by interpolating data on a regular Cartesian grid and in particular using the projected coordinate reference system (CRS) EPSG:3004 (European Petroleum Survey Group, https://epsg.org/home.html), also named "Monte Mario / Italy zone 2 - Datum: Roma 40 - Projection: Gauss-Boaga - Zone: East". The area of use for EPSG:3004 is Italy - East of 12° onshore and offshore. The proposed processing chain was designed to save output radar products in Geographic Tagged Image File Format (GeoTiff, https://www.ogc.org/standard/geotiff) so that any geographical information system (GIS) software can easily ingest them. GeoTiff standard requires metadata providing projection information for the exchange of

georeferenced and geocoded imagery so we chose EPSG:3004 as projected CRS for output radar products related to Central Eastern Italy.
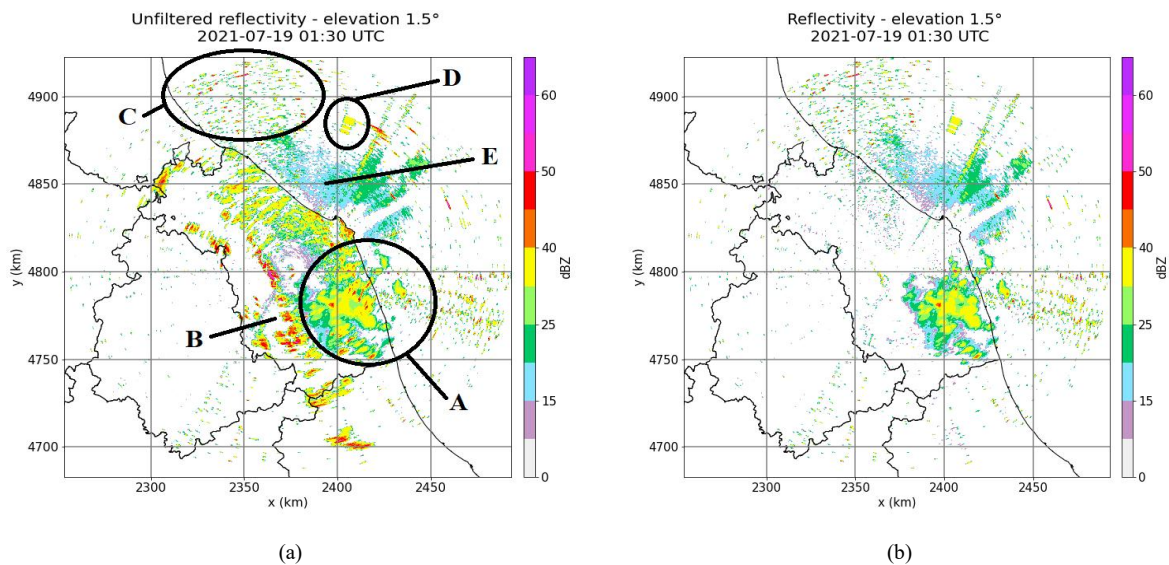
Figure 5. Unfiltered horizontal reflectivity (UZ$_H$) measured on 2021-07-19 at 01:30 UTC at elevation 1.5° in presence of precipitation (a) and the corresponding reflectivity Z$_H$ Doppler-filtered by Eldes (b). Labels refer to weather features (A), ground clutter (B), interferences (C), Racon echoes (D) and sea clutter (E).

A scheme of Cingoli radar filtering and processing chain is shown in Figure 6. The processing chain is divided into four main sections: residual ground clutter filtering, attenuation correction, separation of meteorological from non-meteorological targets and removal of Racon echoes. The processing chain receives as input an HDF5 file with the entire polar radar volume and it starts working on Doppler-filtered reflectivity (Z) data.


Figure 6. Scheme of Cingoli radar data processing chain.

Before describing in detail the individual steps of the chain, we report the final result obtained by applying the algorithms used for the present work to the previously mentioned case; Figure 7 then shows the VMI (on the left) and the SRI (on the right), two of the outputs of the processing chain, related to 2021-7-19 at 1:30 UTC. SRI is calculated starting from VMI data through the power law proposed by Marshall and Palmer, consistent with an exponential drop-size distribution [13]:

$$Z = a\,R^b \tag{1}$$

where a and b are adjustable parameters while Z and R are the reflectivity factor in mm^6 m^{-3} and the rainfall rate in mm h^{-1}, respectively; according to Marshall and Palmer study, in this work we used a=200 and b=1.6. It is

evident from Figure 7 how the processing chain is able to suppress the various sources of noise while preserving the meteorological signal at the same time.
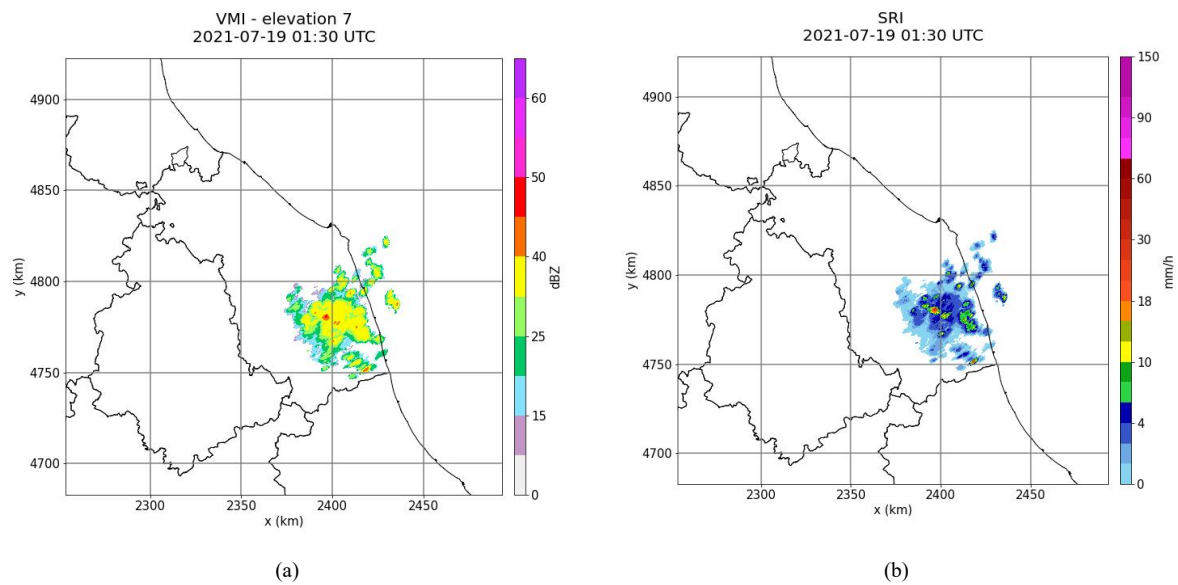
Figure 7. VMI in dBZ (a) and SRI in mm/h (b) as output products of the processing chain related to the presence of precipitation measured on 2021-7-19 at 1:30 UTC.

Figure 8 shows the MSG (Meteosat Second Generation) RGB composite airmass for 2021-7-19 at 1:30 UTC (the same time as Figure 7). Furthermore, maximum rainfall intensity data coming from the regional meteorological and hydrological monitoring network (SIRMIP) and measured every 15 minutes, confirm that on 2021-7-19 at 1:30 UTC the only measured values greater than 0 mm per minute are related to rain gauges located in the South of Marche region. SIRMIP is managed by Marche Region Civil Protection Service [14] making data freely available through the SIRMIP on-line (SOL) web application at http://app.protezionecivile.marche.it/sol [15].
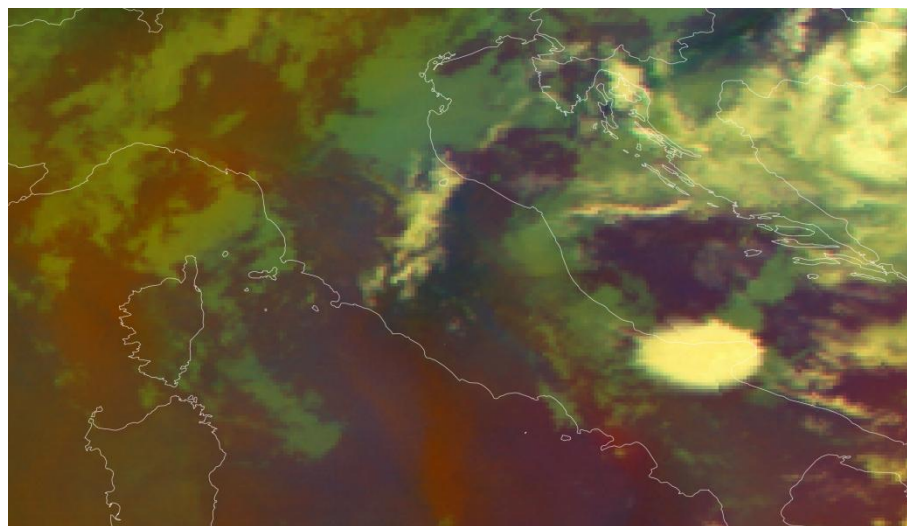
**Figure 8.** MSG RGB composite airmass related to 2021-7-19 at 1:30 UTC.

4. Ground Clutter

Weather radars are often installed on the top of a hill or a mountain, with the purpose of surveillance of complex-orography territories; this is also the case of Cingoli radar, installed at about 750 meters on the Apennine chain. Since a radar scan from a high site can imply a large number of pixels affected by ground-clutter, its rejection is then essential for the use of radar data, both for quantitative and qualitative purposes. The

texture-based technique proposed by Gabella and Notarpietro [16] and used in the present work is based on the fact that non-stationary ground clutter and anomalously propagated echoes decorrelate rapidly in space and are spatially heterogeneous. The signature of such echoes may be recognized in reflectivity data, as their spatial variability is larger than the weather echoes. The filtering technique focuses on the horizontal spatial variability of the radar reflectivity field. Gabella algorithm can be divided into two logical parts: the first part consists of a spatial-proximity filter and the second is a test of compactness. The former is a consequence of the larger spatial continuity of precipitation fields than ground clutter, and the latter of the different spatial characteristics of residual clutter and anomalously propagated echoes with respect to precipitation field. The first filter is applied to each pixel in order to eliminate data that are weakly spatially correlated to the surrounding ones. For this purpose, a square window of side length w_{size} pixel around the considered polar bin was used. The reflectivity value of the pixel is assumed to be a meteorological echo when the differences between it and n_p surrounding pixels in the window are below a certain threshold Tr_1; otherwise, the pixel is considered to be affected by ground clutter and a flag replaces its value. The second filter identifies a minimum echo area considering adjacent pixels of not null intensity: the pixels are considered to belong to the same group if they touch on any of the eight possible directions (including diagonal directions). The ratio R_p of the total number of pixels in the group and the number of pixels defining its boundary is evaluated for each group and a given group is classified as unwanted clutter when R_p is less than a minimum threshold Tr_2. As suggested by Gabella, for this work we used the following value for the filters: $w_{size} = 5$, $Tr_1 = 6$ dBZ, $n_p = 8$ and $Tr_2 = 1.3$. The choice of Tr_2 implies that the smallest compact group accepted as a meteorological feature must have more than 11 pixels.

In order to show the performance of the processing chain in its steps, the polar volume measured by the Cingoli radar on 2022-6-15 at 16 UTC will be considered. During that day, Italy was positioned on the eastern edge of a high-pressure area on which northwesterly currents flow at high altitude. On the ground, the baric gradient is very low and the circulation follows the regime of sea breezes that, combined with daytime heating, contribute to the formation of cumulus clouds on the Apennine ridge in the early afternoon.

Forecasted vertical profile data from European Centre for Medium-Range Weather Forecasts (ECMWF, https://www.ecmwf.int) and reported in Figure 9 for 2022-6-15 at 12 UTC shows a low predisposition to deep convection due the high level of free convection, so only some cumulus clouds evolved in severe storm. In particular, an intense storm system remained stationary upon Umbria region and northwest of Marche region, bringing heavy rains from 14:45 to 17:00 UTC. In Figure 10, the MSG HRV (High Resolution Visible) RGB composite is reported for 2022-6-15 at 16 UTC.
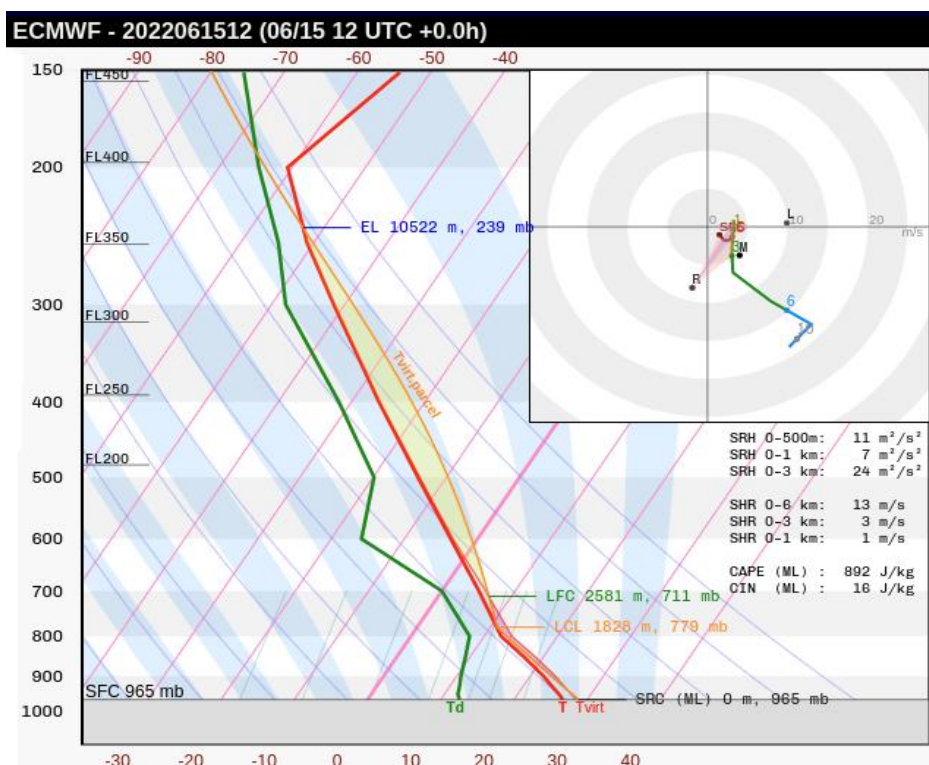

Figure 9. Forecasted vertical profile data for 2022-6-15 at 12 UTC from ECMWF. T_d and T_{virt} represent dew point and virtual temperature, respectively.
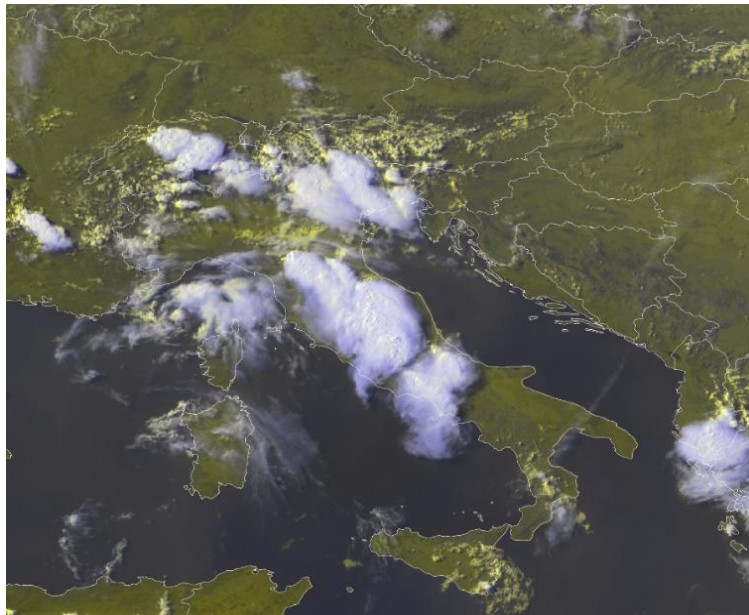
Figure 10. MSG HRV (High Resolution Visible) RGB composite related to 2022-6-15 at 16 UTC.

Figure 11 shows the reflectivity Doppler-filtered by Eldes (input of the processing chain, on the left) at elevation 0° and the reflectivity filtered according to the Gabella algorithm for residual ground clutter removal (right). It is evident from right side of Figure 11 how the Gabella filter is able to remove the clutter echoes present in the left side of Figure 11 and especially in the northeastern quadrant.

| (a) | (b) |
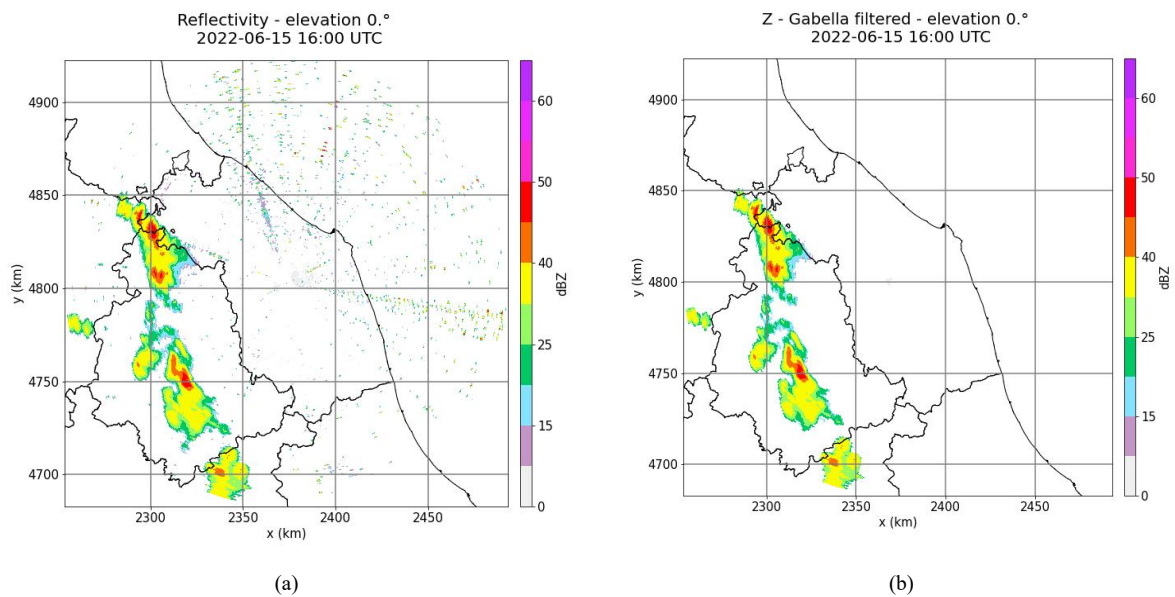
Figure 11. Reflectivity Doppler-filtered by Eldes (left) measured on 2022-6-15 at 16 UTC (elevation 0°) and the reflectivity filtered according to the Gabella algorithm for residual ground clutter removal (right).
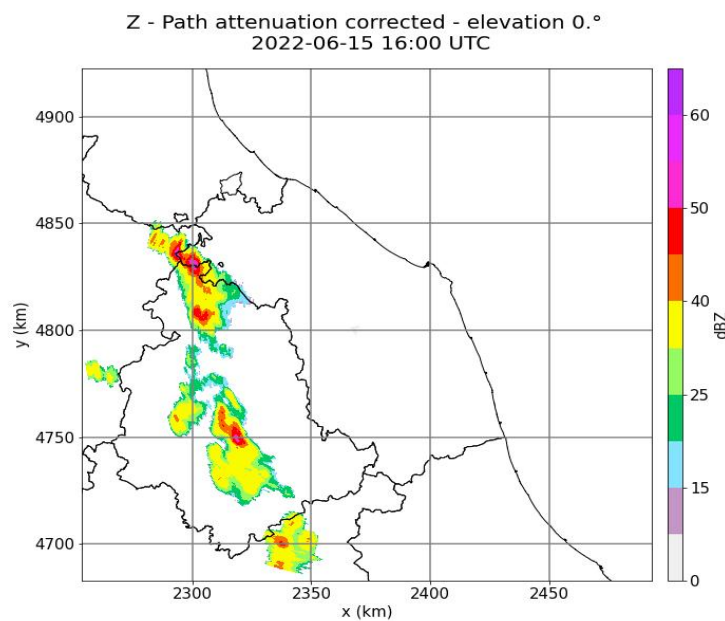
5. Attenuation Correction

Radar data was gate-by-gate corrected for the attenuation using the iterative approach of Jacobi and Heistermann [17] that represents a modification of the algorithm proposed by Kraemer and Verworn [18]. The algorithm used aims at finding the optimal combination of the parameters c and d that relate the specific attenuation k (in dB/km) and radar reflectivity Z via a power law:

$$k = c\,Z^{d} \tag{2}$$

The optimization process started with a couple of initial values for linear coefficient c and exponential coefficient d, i.e. c_{max} and d_{max}. The coefficients are then successively reduced for contiguous beam sectors to minimal allowed values c_{min} and d_{min} until stability is achieved. The algorithm also fixed the number of iterations c_n between c_{max} and c_{min} and d_n between d_{max} and d_{min}. As a criterion to detect instability, the attenuation correction along a beam is considered as unstable if the value of attenuation-corrected reflectivity in any gate exceeded a maximum value $Z_{corr.max}$ or if the path-integrated attenuation (PIA) exceeds a maximum value PIA_{max}.

For the present work we used the following values: $c_{max} = 1.67 \ 10^{-4}$, $c_{min} = 2.33 \ 10^{-5}$, $c_n = 4$, $d_{max} = 0.7$, $d_{min} = 0.65$, $d_n = 6$, $Z_{corr.max} = 59$ dBZ and $PIA_{max} = 20$ dB; furthermore, as reported in Table 2, gate resolution of Cingoli radar data is 125 m. The attenuation-corrected reflectivity according to the Jacobi and Heistermann algorithm is shown in Figure 12; as can be observed, reflectivity values related to convective cells are increased with respect to the right side of Figure 11, i.e., after the application of Gabella filter.

Figure 12. Attenuation-corrected reflectivity related to radar data measured on 2022-6-15 at 16 UTC (elevation 0°).
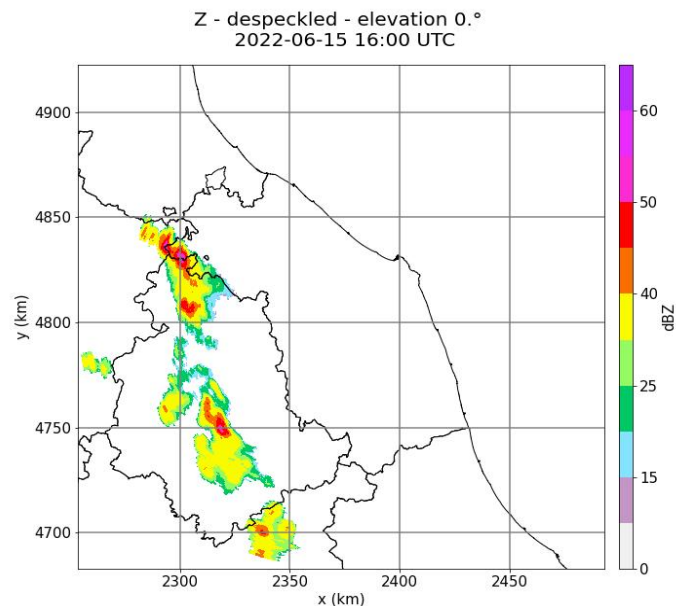
6. Separation and Removal of Non-meteorological Targets

In order to separate meteorological from non-meteorological features in radar data and therefore be able to discard the latter, we decided to implement the methodology proposed by Kilambi et al. [19] in the framework of the processing chain described here. The methodology is based on a commonly observed property of meteorological targets compared to other targets, i.e. they present simultaneously high values of correlation coefficient (ρ_{HV}) and values of differential reflectivity (Z_{DR}) close to 1 in linear units. In other words, meteorological targets are basically uniform in shape and close to spherical. Starting from ρ_{HV} and Z_{DR} data measured by dual-polarization systems such as Cingoli radar, depolarization ratio (DR) can be derived:

$$DR = \left(Z_{DR} + 1 - 2 \, Z_{DR}^{1/2} \, \rho_{HV} \right) / \left(Z_{DR} + 1 + 2 \, Z_{DR}^{1/2} \, \rho_{HV} \right) \tag{3}$$

where Z_{DR} and DR are in linear units. DR has values between 0 and 1 but we converted into decibel (dB) units for the implementation of the algorithm. According to Kilambi et al., non-meteorological radar echoes are characterized by values of DR > −12 dB and reflectivity Z < 35 dBZ. This simple method has proven effective for identifying non-meteorological targets at C- as well as at X-band, so we used it for Cingoli radar data. Since we measured echoes from light rain having reflectivity values of about 15 dBZ, a less stringent condition for the reflectivity (Z < 15 dBZ) was adopted for this work. Misclassifications between weather and non-meteorological echoes are typically caused by isolated pixels in the melting layer or at the edge of echo patterns

[19] then, as suggested by Kilambi et al., we adopted a despeckling algorithm in order to reduce such misclassifications. A window of width 3 around the pixel has been used for despeckling. In Figure 13 the reflectivity related to radar data measured on 2022-6-15 at 16 UTC (elevation 0°) is reported after removal of non-meteorological targets by means of depolarization ratio and despeckling. The effect of such algorithms is not so evident from the Figure because they are devoted to isolated pixels, operating in cascade to two other filters, Doppler by Eldes and Gabella, all aimed at removing non-meteorological from meteorological echoes. It is nevertheless important to point out that, as expected, applying depolarization ratio and despeckling algorithms preserves all meteorological features present in radar data.

Figure 13. Reflectivity related to radar data measured on 2022-6-15 at 16 UTC (elevation 0°) after removal of non-meteorological targets.

Ground clutter filtering, attenuation correction and algorithm for separation of meteorological from non-meteorological targets were applied to the reflectivity of each elevation of the radar volume.

7. Racon Filtering

Randomly, Cingoli radar data present a strong echo from the Adriatic Sea most likely due to a Racon. A Racon is a radar transponder commonly used for maritime navigation to mark hazards; when a Racon receives a radar pulse, it responds with a user-programmed signal at the same frequency placing a characteristic signature on the radar display (see label D North-East from radar site on Figure 5). In its normal operation, a Racon is activated by X-band radars present on ships as an aid to navigation.
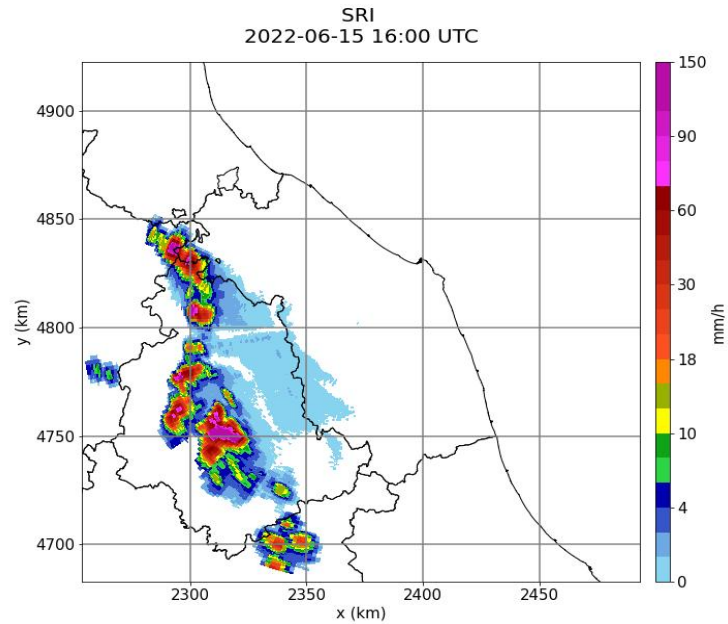
Echoes from Racon are observable on Cingoli radar data at the first two elevations only and they always appear in the same geographical position at both elevations. In polar coordinates, Racon echoes have been identified in the area bounded by azimuth between 17 and 23 degrees and range bin between 657 and 734 (i.e., between 82.125 and 91.75 km away from the radar site). The echoes from Racon can appear by chance at both elevations or in only one of the two; however, it is eliminated or at least reduced by means of the filter created ad-hoc for the present work.

We have assumed that echoes outside the identified area are not affected by Racon so we focused our attention only on radar bins within the Racon area and belonging to the first three elevations.

Basically, for each pixel with a valid reflectivity value present in the Racon area and in the selected elevations, the corresponding pixels along its vertical are examined; if at least a pixel has a not valid reflectivity value then the pixel under examination is classified as affected by Racon and then discarded. Removal of Racon echoes is evident from VMI related to data measured on 2021-7-19 at 1:30 UTC and shown in Figure 7 compared to unfiltered and Doppler-filtered reflectivity in Figure 5.

In Figures 14 and 15, the SRI and the three-dimensional VMI related to radar data measured on 2022-6-15 at 16 UTC are shown as output of the processing chain. The vertical structure of the precipitating system up to 12.5 km is clearly visible from Figure 15, obtained by interpolating polar coordinates of all elevations into EPSG:3004 Cartesian grid with horizontal and vertical resolution of 125 m and 500 m, respectively.

Real-time VMI and SRI, two of the outputs of the processing chain described here, are available online at Marche Region Civil Protection Service webpage http://console.protezionecivile.marche.it/MonitoraggioMeteo/ observations/radar/html/radar.html.

Figure 14. SRI in mm/h related to Cingoli radar data measured on 2022-6-15 at 16 UTC as output of the processing chain.
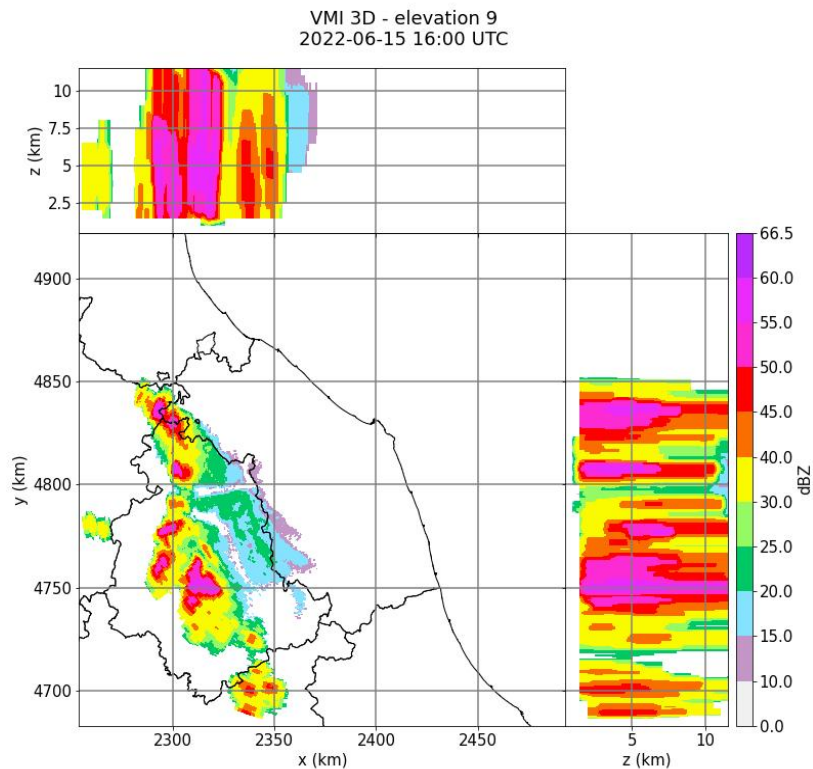
Figure 15. Three-dimensional VMI in dBZ related to Cingoli radar data measured on 2022-6-15 at 16 UTC as output of the processing chain.

8. Conclusion

In this work a data-processing chain developed ad hoc in order to deal with the sources of error affecting Cingoli X-band weather radar data has been presented in detail. The software was written using open source technology and is operationally used by the Civil Protection Service of Marche Region, Italy. The processing chain has been found to be able to greatly reduce or even suppress the unwanted radar echoes while preserving meteorological features at the same time. The performance of the data-processing chain has been evaluated in the light of case studies related to meteorological events that recently interested Marche region territory.

Cingoli radar data present clutter echoes received from the Adriatic Sea at the first two elevations of the scan. Measured Doppler velocity pattern due to sea clutter is similar to that due to the presence of moderate rainfall so Doppler filtering cannot work properly. Furthermore, operational and research weather radars are often covered by a radome that serves several purposes such as protecting the antenna and pedestal from weathering, providing a consistent environment and a direction-independent wind load. In addition to these technical reasons, radomes also mitigate the visual impact of operational weather radars by hiding the moving parts. Despite all this, radomes have also the deleterious effect of disrupting the transmitted and received radar signals; in particular, rain and ice on the radome degrade the signals beyond the nominal dry-radome attenuation, accurately measured by the radar vendor. For frequencies below C-band, these impacts can usually be ignored but at higher frequencies, and in particular at X-band, the impact of radome attenuation can be significant.

Since Cingoli radar is about 30 km away from the Adriatic Sea and is covered by a radome, the processing chain described here will be reviewed and updated in a future work in order to take into account the effects of sea clutter and wet radome attenuation on radar data.

Acknowledgment

Conflict of Interest

There is no conflict of interest for this study.

References

[1] Baldini, L.; Chandrasekar, V.; Moisseev, D. Microwave radar signatures of precipitation from S band to Ka band: application to GPM mission *Eur. J. Remote. Sens.* **2012**, *45*, 75–88, https://doi.org/10.5721/EuJRS2012 24508.

[2] Yoon, S.-S.; Lim, S.-H. Analyzing the Application of X-Band Radar for Improving Rainfall Observation and Flood Forecasting in Yeongdong, South Korea. *Remote. Sens.* **2022**, *14*, 43, https://doi.org/ 10.3390/rs1401 0043.

[3] WMO. Meteorological Radar at the World Radiocommunication Conference, Meteoworld March 2015. Available online: https://public.wmo.int/en/resources/meteoworld/meteorological-radar-world-radiocommunication-conference (accessed on 16 March 2023).

[4] Anagnostou, M.N.; Kalogiros, J.; Anagnostou, E.N.; Tarolli, M.; Papadopoulos, A.; Borga, M. Performance evaluation of high-resolution rainfall estimation by X-band dual-polarization radar for flash flood applications in mountainous basins. *J. Hydrol.* **2010**, *394*, 4–16, https://doi.org/10.1016/j.jhydrol.2010.06.026.

[5] Hosseini, S.H.; Hashemi H.; Berndtsson, R.; South, N., Aspegren, H.; Larsson, R.; Olsson, J.; Persson, A.; Olsson, L. Evaluation of a new X-band weather radar for operational use in south Sweden. *Water Sci. Technol.* **2020**, *81*, 1623–1635, https://doi.org/10.2166/wst.2020.066.

[6] Antonini, A.; Melani, S.; Corongiu, M.; Romanelli, S.; Mazza, A.; Ortolani, A.; Gozzini, B. On the Implementation of a Regional X-Band Weather Radar Network. *Atmosphere* **2017**, *8*, 25, https://doi.org/10.3390/atmos8020025.

[7] i Ventura, J.F.; Lainer, M.; Schauwecker, Z.; Grazioli, J.; Germann, U. Pyrad: A Real-Time Weather Radar Data Processing Framework Based on Py-ART. *J. Open Res. Softw.* **2020**, *8*, 28, https://doi.org/10.5334/jors.330.

[8] Heistermann, M.; Collis, S.; Dixon.; M.J.; Giangrande, S.; Helmus, J.J.; Kelley, B.; Koistinen, J.; Michelson, D.B.; Peura, M.; Pfaff, T.; et al. The emergence of open-source software for the weather radar community. *Bull. Am. Meteorol. Soc.* **2015**, *96*, 117–128, https://doi.org/10.1175/BAMS-D-13-00240.1.

[9] Michelson, D.; Henja, A.; Ernes, S.; Haase, G.; Koistinen, J.; Ośródka, K.; Peltonen, T.; Szewczykowski, M.; Szturc, J. BALTRAD advanced weather radar networking. *J. Open Res. Softw.* **2018**, *6*, 12, https://doi.org/10.5334/jors.193.

[10] Heistermann, M.; Jacobi, S.; Pfaff, T. Technical Note: An open source library for processing weather radar data (wradlib). *Hydrol. Earth Syst. Sci.* **2013**, *17*, 863–871, https://doi.org/10.5194/hess-17-863-2013.

[11] Helmus, J.J.; Collis, S.M. The Python ARM radar toolkit (Py-ART), a library for working with weather radar data in the python programming language. *J. Open Res. Softw.* **2016**, *4*, 25, https://doi.org/10.5334/jors.119.

[12] Saltikoff, E.; Haase, G.; Delobbe, L.; Gaussiat, N.; Martet, M.; Idziorek, D.; Leijnse, H.; Novák, P.; Lukach, M.; Stephan, K. OPERA the Radar Project. *Atmosphere* **2019**, *10*, 320, https://doi.org/10.3390/atmos10060320.

[13] American Meteorological Society (AMS). Glossary of Meteorology: Marshall–Palmer relation. Available online: https://glossary.ametsoc.org/wiki/Marshall-palmer_relation (accessed on 16 March 2023).

[14] Marche Region. Security and Civil Protection Service (in Italian). Available online: http://www.regione.marche.it/Regione-Utile/Protezione-Civile (accessed on 16 March 2023).

[15] Pellegrini, M. Dissemination and Exploitation of Regional Meteo-Hydrological Datasets through Web-based Interactive Applications: The SOL System Case Study. *Online J. Eng. Sci.* **2021**, *1*, 19–28, https://doi.org/10.31586/ojes.2021.180.

[16] Gabella M.; Notarpietro, R. Ground clutter characterization and elimination in mountainous terrain. In Use of radar observations in hydrological and NWP models. *Proceedings of ERAD* **2002**, *305*, 305–311, https://iris.polito.it/handle/11583/1411995.

[17] Jacobi S.; Heistermann M. Benchmarking attenuation correction procedures for six years of single-polarised C-band weather radar observations in south-west Germany. Geomat. *Nat. Haz. Risk* **2016**, *7*, 1785–1799, https://doi.org/10.1080/19475705.2016.1155080.

[18] Kraemer S.; Verworn H. R. Improved C-band radar data processing for real time control of urban drainage systems. In proceedings of the 11th International Conference on Urban Drainage, Edinburgh, Scotland, 31 August – 5 September 2008.

[19] Kilambi A.; Fabry F.; Meunier V. A Simple and Effective Method for Separating Meteorological from Nonmeteorological Targets Using Dual-Polarization Data. *J. Atmospheric Ocean. Technol.* **2018**, *35*, 1415–1424, https://doi.org/10.1175/JTECH-D-17-0175.1.